STEM CELLS®

TISSUE-SPECIFIC STEM CELLS

IGF-1-Mediated Osteoblastic Niche Expansion Enhances Long-Term Hematopoietic Stem Cell Engraftment After Murine Bone Marrow Transplantation

ANNA CASELLI,[a,b] TIMOTHY S. OLSON,[b,c,d] SATORU OTSURU,[b] XIAOHUA CHEN,[b] TED J. HOFMANN,[b] HYUN–DUCK NAH,[e] GIULIA GRISENDI,[a] PAOLO PAOLUCCI,[a] MASSIMO DOMINICI,[a] EDWIN M. HORWITZ[b,d]

[a]Department of Medical and Surgical Sciences of Children & Adults, University Hospital of Modena and Reggio Emilia, Modena, Italy; [b]Division of Oncology, [c]Division of Hematology, and [d]Department of Pediatrics, Perelman School of Medicine, The University of Pennsylvania, Philadelphia, Pennsylvania, USA; [e]Division of Plastic and Reconstructive Surgery, The Children's Hospital of Philadelphia, Philadelphia, Pennsylvania, USA

Key words: Stem cell transplantation • Niche • Osteoblasts • Insulin-like growth factor 1 • Mouse

ABSTRACT

The efficiency of hematopoietic stem cell (HSC) engraftment after bone marrow (BM) transplantation depends largely on the capacity of the marrow microenvironment to accept the transplanted cells. While radioablation of BM damages osteoblastic stem cell niches, little is known about their restoration and mechanisms governing their receptivity to engraft transplanted HSCs. We previously reported rapid restoration and profound expansion of the marrow endosteal microenvironment in response to marrow radioablation. Here, we show that this reorganization represents proliferation of mature endosteal osteoblasts which seem to arise from a small subset of high-proliferative, relatively radio-resistant endosteal cells. Multiple layers of osteoblasts form along the endosteal surface within 48 hours after total body irradiation, concomitant with a peak in marrow cytokine expression. This niche reorganization fosters homing of the transplanted hematopoietic cells to the host marrow space and engraftment of long-term-HSC. Inhibition of insulin-like growth factor (IGF)-1-receptor tyrosine kinase signaling abrogates endosteal osteoblast proliferation and donor HSC engraftment, suggesting that the cytokine IGF-1 is a crucial mediator of endosteal niche reorganization and consequently donor HSC engraftment. Further understanding of this novel mechanism of IGF-1-dependent osteoblastic niche expansion and HSC engraftment may yield clinical applications for improving engraftment efficiency after clinical HSC transplantation. STEM CELLS *2013;31:2193–2204*

Disclosure of potential conflicts of interest is found at the end of this article.

INTRODUCTION

Adequate donor stem cell engraftment is essential to achieve successful bone marrow transplantation (BMT). The capacity for donor hematopoietic stem cells (HSCs) to engraft within host bone marrow (BM) depends on their interactions with specific microenvironments designated as HSC niches [1–3]. Under homeostatic conditions, BM niches nurture HSCs, maintaining the critical balance of quiescence, self-renewal, and differentiation [4,5]. After BMT, donor HSC must home to and engraft within these niches and then markedly expand to repopulate the pool of primitive hematopoietic cells within host marrow, ultimately restoring the homeostatic milieu [6]. Thus, the relationship of HSC's with these niches is an intricate and dynamic interaction [7].

Many recent studies have attempted to identify the cellular components and complex regulatory networks governing HSC niche function [6,8,9]. Osteoblasts have been described as a pivotal cellular component of the endosteal, or osteoblastic niche [4,5,10]. Osteoblasts are known to support hematopoiesis in vitro [11,12]. Moreover, in situ depletion of osteoblasts severely diminishes BM hematopoiesis [13]. At homeostasis, many HSCs reside along the single layer of osteoblasts that comprises the endosteal surface, and following BMT, HSCs have been reported to localize to this endosteal region [14,15]. Although other cellular

Author contributions: A.C. and T.O.: collection of data, data analysis and interpretation, and manuscript writing; S.O.: Collection of data and data analysis and interpretation; X.C., T.H., and G.G.: collection and assembly of data; H.-D.N.: design and provision of study material; P.P.: conception and design; M.D.: conception, design, data analysis and interpretation, manuscript writing, and final approval of manuscript; E.H.: oversaw entire project, conception, design, data analysis and interpretation manuscript writing, and final approval of manuscript. A.C. and T.S.O. contributed equally to this article.

MD and EMH are co-senior authors.

Correspondence: Edwin M. Horwitz, M.D., Ph.D., The Children's Hospital of Philadelphia, Colket Translation Research Building #3010, 3501 Civic Center Boulevard, Philadelphia, Pennsylvania 19104, USA. Telephone: 215-590-5476; Fax: 215-590-3770; e-mail: horwitze@email.chop.edu; or Massimo Dominici, M.D., Department of Medical and Surgical Sciences, University of Modena & Reggio Emilia, Via del Pozzo, 71, Modena 41100, Italy. Telephone: +39-059-422-2858; Fax: +39-059-422-3341; e-mail: massimo.dominici@unimore.it Received March 24, 2013; accepted for publication May 29, 2013; first published online in STEM CELLS *EXPRESS* July 2 2013. 1066-5099/2013/$30.00/0 doi: 10.1002/stem.1463

elements such as endothelial cells also play key roles in HSC niche function [9], these data suggest a critical role for osteoblasts in supporting HSCs both during homeostasis and after BMT.

We recently described a remarkable cellular remodeling of the marrow architecture after hematopoietic cell ablation with total body irradiation (TBI) in mice [16]. Marrow radioablation initiates a program of striking endosteal osteoblast expansion, accompanied by relocalization of surviving marrow elements, particularly megakaryocytes, to the expanded endosteal surface. Endosteal expansion is accompanied by significantly increased levels of stromal cell-derived factor (SDF)-1, a critical regulator of HSC interactions with the osteoblastic niche [17]. However, our prior study did not investigate the functional significance of this cellular remodeling in facilitating the complex process of HSC homing and engraftment. Additionally, the specific cellular and molecular pathways required for the remodeling response were not defined.

Here, we present data suggesting that post-TBI endosteal cell expansion fosters donor hematopoietic cell homing to the marrow space as well as short- and long-term (LT) hematopoietic reconstitution. Moreover, insulin-like growth factor 1 (IGF-1), a known natural agonist of osteoblast growth and proliferation [18], appears to be a critical regulator of marrow remodeling and donor HSC engraftment. Collectively, our data provide mechanistic evidence that the dynamic structural reorganization of the osteoblastic niche following marrow radioablation is vital for HSC engraftment and durable hematopoietic recovery post-transplantation.

Materials and Methods

Animal Use and Care

All procedures were performed in accordance with protocols approved by The Children's Hospital of Philadelphia Institutional Animal Care and Use Committee. Six- to twelve-week-old C57BL/6 wild-type (WT) mice were purchased from Jackson Laboratories (Bar Harbor, ME, http://www.jax.org). Transgenic C57BL/6 mice expressing green fluorescent protein (GFP) under control of the H2K promoter (H2K-GFP) [19] were used as GFP^+ BM donors in transplantation experiments. pOBCol2.3GFPemd (COL2.3GFP) mice [20,21] were generously provided by Dr. David Rowe (University of Connecticut; Farmington, CT). Animals were housed under specific pathogen-free conditions.

Osteoblast Niche Expansion Studies

For irradiation experiments, animals received myeloablative TBI (1,125 cGy) via an x-ray source (X-RAD 320: Precision X-Ray Inc.; North Branford, CT, http://www.pxinc.com). To assess osteoblastic niche changes post-TBI, WT or Col2.3GFP mice were irradiated and then euthanized at specified time points after TBI (30 minutes; 3, 6, 12, 18, 24, 48, 72, 96 hours; $n = 10$ per group). Mice not receiving TBI were used as comparison groups. In a subset of experiments, irradiated mice received intraperitoneal (i.p.) 50 mg/kg injections of BrdU (BD Biosciences; San Diego, CA, http://www.bdbiosciences.com) 1 hour prior to euthanasia except for time point analyses >24 hours post-TBI, when BrdU was given 24 hours prior to euthanasia.

For histology and immunohistochemistry studies, femurs and tibias were fixed in 10% formalin, decalcified for 3–5 days (Regular Cal•Immuno; BBC Biochemical; Stanwood, WA, http://www.bbcus.com) and paraffin-embedded or decalcified for 3 weeks in 15% EDTA before preparing frozen sections using O.C.T. compound (Sakura; Torrence, CA, http://www.sakuraamericas.com). For assessment of osteoblast proliferation and individual osteoblast thickness, sections were stained with hematoxylin and eosin (H+E) (Sigma-Aldrich; St. Louis, MO, http://www.sigmaaldrich.com), and semiquantitatively assessed in blinded fashion to determine the osteoblast score index, representing the average number of endosteal lining cell layers per section. At least five sections/mouse were scored and averaged to provide an individual mouse score. Osteoblast thickness was assessed by microscopic measurement (three sections/mouse) using the AxioVision 4.5 SP1 software (Carl Zeiss, Thornwood, NY, http://corporate.zeiss.com).

Immunostaining for BrdU, Ki-67, GFP, and IGF-1 was performed using rat anti-BrdU antibody (1:50) (Roche; Mannheim, Germany, https://www.roche-applied-science.com), rabbit anti-Ki67 antibody (Abcam; Cambridge, MA, http://www.abcam.com), rabbit anti-GFP antibody (Invitrogen; Carlsbad, CA, http://www.invitrogen.com), and rabbit anti-IGF1 antibody (Abbiotec; San Diego, CA, http://www.abbiotec.com) along with goat anti-rat/rabbit biotinylated secondary antibody (1:180), avidin/biotin complexes, and NovaRED peroxidase development (Vector Laboratories; Burlingame, CA, http://www.vectorlabs.com). Target-specific staining was verified by performing negative control staining with rabbit and rat isotype control primary antibodies (Vector, BD Biosciences). Slides were examined using a Zeiss Axiovert 200M (Carl Zeiss) with either a 10×/0.25NA or a 40×/0.6NA dry objective. All photomicrographs were acquired with the attached AxioCam HR color camera and analyzed using AxioVision 4.5 SP1 software (Carl Zeiss).

To assess ex vivo primary osteoblast growth and colony formation from pre- and post-TBI mice, BM was flushed from femurs, and the endosteal bone surface was denuded by vigorous scraping using a 26 g needle. Denudation of the endosteal lining cells was confirmed by histologic analysis (Supporting Information Fig. S1). The resulting cell suspension was plated in osteoblast growth media (50/50 Dulbecco's modified Eagle's medium/F-12 with 10% fetal bovine serum, glutamate, pen/strep, and 25 μg/ml ascorbic acid) for 7 days. Plates were then washed with plain phosphate buffered saline, and adherent cells were fixed to the plate in 4% paraformaldehyde, permeabilized with 0.1% Triton X-100, and immunostained for osteocalcin expression using a rabbit-anti-mouse osteocalcin polyclonal antibody (Takara Bio Inc.; Otsu, Japan, http://www.clontech.com/takara), a biotinylated secondary anti-rabbit antibody, avidin-biotin complexes, and 3,3′-Diaminobenzidine substrate (Vector). Numbers and size (diameter) of osteocalcin positive colonies were counted using the Zeiss Axiovert (Carl Zeiss).

Growth Factor Expression Analyses

To assess BM growth factor expression, femurs from euthanized pre- and post-TBI mice were collected, and marrow was flushed with phosphate buffered saline using a 26 g needle. For protein analysis, BM was flushed with 1 ml of phosphate buffered saline containing protease inhibitor (Roche), followed by addition of Nonidet P-40 (United States Biological; Swampscott, MA, http://www.usbio.net) (1%, vol/vol). Cells were lysed by freeze/thaw three times, and cell debris removed by centrifugation at 14,000g for 5 minutes. Platelet-derived growth factor-BB (PDGF-BB), transforming growth factor beta (TGFβ), basic fibroblast growth factor (bFGF), SDF-1, and IGF-1 protein concentrations were measured by ELISA (R&D Systems; Minneapolis, MN, http://www.rndsystems.com) according to manufacturer's instructions.

For quantitative PCR (qPCR) analysis, total RNA was isolated from flushed BM cells using TRIzol Reagent (Invitrogen). First-strand cDNA was synthesized using the High-Capacity cDNA Reverse Transcription Kit (Applied Biosystems; Foster City, CA, http://www.appliedbiosystems.com), per manufacturer's protocol. qPCR (7500 Fast Real-Time PCR System, Applied Biosystems) was performed using target-specific primers (Supporting Information Table S1) and SYBR Green PCR Master Mix system (Applied Biosystems). Glyceraldehyde 3-phosphate dehydrogenase expression was used to normalize for RNA input. Reaction

conditions for amplification were: 95°C for 10 minutes, then 50 cycles of: 95°C for 15 seconds and 55°C–60°C for 60 seconds. All samples were measured in duplicate.

Homing and Transplantation Studies

For BMT studies, whole BM from transgenic mice with pancellular expression of GFP under the control of the H2K promoter (H2K-GFP) [19] or Sca-1-depleted BM from syngeneic WT mice was injected into the lateral tail vein at a dose of 3×10^6 cells per recipient. Sca-1 depletion was performed by sorting the 7-amino-actinomycin D^- Sca-1^- fraction from whole BM (Supporting Information Fig. S2), using a FACSAria III cell sorter (BD Biosciences).

BM was infused either immediately (0-hour), 24 hours, or 48 hours after recipient irradiation (1,125 cGy). In initial homing studies, BM was collected 6 or 24 hours after transplant, red blood cells (RBCs) were lysed, and BM was stained with propidium iodide and assessed by flow cytometry for the percentage of live BM cells expressing GFP. All flow cytometry experiments were performed on a FACSCalibur with Cellquest software or FACSAria cell sorter with FACSDiva software (BD Biosciences).

Competitive repopulation secondary transplantation assays were performed as follows. Three cohorts (six mice/cohort) of WT mice received 3×10^6 GFP BM cells 30 minutes, 24 hours, or 48 hours post-TBI. Twenty-four hours after primary BMT, primary recipients were euthanized, and all BM from bilateral femurs and tibias were collected and pooled within each cohort. Using a previously defined dosing scheme in which all bilateral femur and tibia BM represents a 25% BM equivalent (BME) dose [22], a 12.5% BME dose derived from each of the primary recipient groups was injected into three separate groups of WT secondary recipient mice ($n = 10$/group) irradiated 24 hours prior to secondary BMT. Each secondary recipient also received 2×10^5 whole BM cells from an unirradiated WT mouse, serving as a competitor HSC population. Three to eighteen weeks after secondary transplantation, secondary recipients were analyzed by flow cytometry for GFP^+ cell reconstitution in peripheral blood lineages, including RBCs and platelets determined by forward and side scatter, along with myeloid cell, T-cell, and B-cell populations defined by staining with anti-mouse Gr1 (clone RB6-8C5), CD3e (clone 1452c11), and B220 (clone RA36B2) antibodies (BD Biosciences).

IGF-1 Signaling Blockade

To assess the contribution of IGF-1 to niche proliferation and function following irradiation, we treated irradiated WT C57BL/6 mice with i.p. injection of either the IGF-1 receptor tyrosine kinase inhibitor picropodophylin (PPP, 20 mg/kg per dose, Calbiochem: EMD Biosciences Inc.; San Diego, CA, http://www.emdmillipore.com) or vehicle alone (dimethyl sulfoxide/oil, 9:1) at the time of and 12 hours after TBI. At 48 hours post-TBI, mice were euthanized and assessed for osteoblast proliferation as above. A second cohort of irradiated mice ($n = 6$/group) that were untreated, PPP-treated, or sham-treated received 3×10^6 GFP^+ BM cells 48 hours post-TBI and were then assessed as distinct primary recipient cohorts for relative HSC engraftment efficiency by competitive secondary transplant assay, as detailed above.

Statistical Methods

Data are presented as mean ± SD. Data were analyzed by two-tailed Student's t test for mean comparisons, by Fisher's Exact test for percent positive comparisons or by one-way analysis of variance (ANOVA) for multiple comparisons. Statistical analyses were performed by Microsoft Excel 2010 (Microsoft; Redmond, WA, http://www.microsoft.com) or Prism, Version 4 (GraphPad Inc.; San Diego, CA, http://www.graphpad.com). Statistical significance was defined as $p < .05$.

Results

Complete Osteoblast Niche Expansion After Marrow Radioablation Requires 48 Hours

We previously demonstrated that marrow radioablation induces an increase in the number of layers of marrow endosteal cells 48 hours post-irradiation [16]. These cell layers consisted of large cells with eccentric nuclei and abundant cytoplasm representing N-cadherin$^+$ osteoblasts and smaller cells with a central nucleus and spindle-shaped body consistent with stromal fibroblasts or other mesenchymal elements. We began this study by defining the time course of osteoblast niche expansion post-irradiation, the cellular composition of this expanded population, and the nature of this proliferation.

We first examined murine BM prior to and at multiple time points after lethal irradiation (1,125 cGy), to determine the time course of endosteal cell proliferation. We used both qualitative examination of sections (Fig. 1A) along with blinded quantitative histologic scoring in which the osteoblast proliferation index equated to the predominant number of endosteal cell layers present (Fig. 1B). Confirming our previous findings, prior to irradiation a single layer of endosteal cells lines the surface of metaphyseal trabecular bone (Fig. 1A, upper left). Endosteal cells formed a single continuous layer of bone-lining cells by 3 hours post-TBI, which remained the predominant endosteal cell configuration through 18 hours (Fig. 1B). As hematopoietic marrow cells began to dissipate, significant expansion of endosteal cells was visualized at 24 hours, corresponding to approximately half-maximal cell expansion (Fig. 1A, upper right and 1B). By 48 hours (Fig. 1A, bottom left and 1B), the endosteal cell expansion reached near-maximal levels, with three to four cell layers lining the endosteal surface ($p < .01$ by one-way ANOVA). No further expansion occurred by either 72 or 96 hours post-TBI, although the endosteal surface remained expanded to three to four layers during this period (Fig. 1A, bottom right and 1B; $p < .01$ by one-way ANOVA). In addition to the increase in cell layers at 48 hours post-TBI, individual cells along the bone surface demonstrated significantly increased cell thickness (2.5-fold; $p = .0001$ by t test) compared to endosteal cells prior to irradiation (Fig. 1C). Interestingly, this finding parallels what has been described for the endosteal compartment stimulated after G-CSF mobilization of HSCs [23], suggesting osteoblast activation following TBI exposure that may alter osteoblast adhesive properties for primitive hematopoietic cells [24].

Expanded Osteoblast Niche Consists of Mature Osteoblasts

The endosteal niche consists of many cell types, including osteoblasts, monocytes, fibroblasts, mesenchymal stromal cells, and other stromal elements [12]. Given the diverse morphology of the expanded population of endosteal cells, we sought to determine which endosteal cells underwent proliferation after marrow radioablation. We examined postradiation endosteal changes in transgenic mice in which GFP was expressed under the control of the *Col1a1* (collagen) 2.3 kb promoter, as GFP expression in this strain is limited to mature osteoblasts and is not present in fibroblasts, other stromal elements, or hematopoietic cells [20,21]. Using immunofluorescence to directly assess GFP expression (Fig. 1D) or through performing immunohistochemistry with an anti-GFP antibody (Fig. 1E), we unequivocally found that the vast majority of endosteal cell expansion 48 hours post-TBI was due to increased numbers of GFP^+ mature osteoblasts.

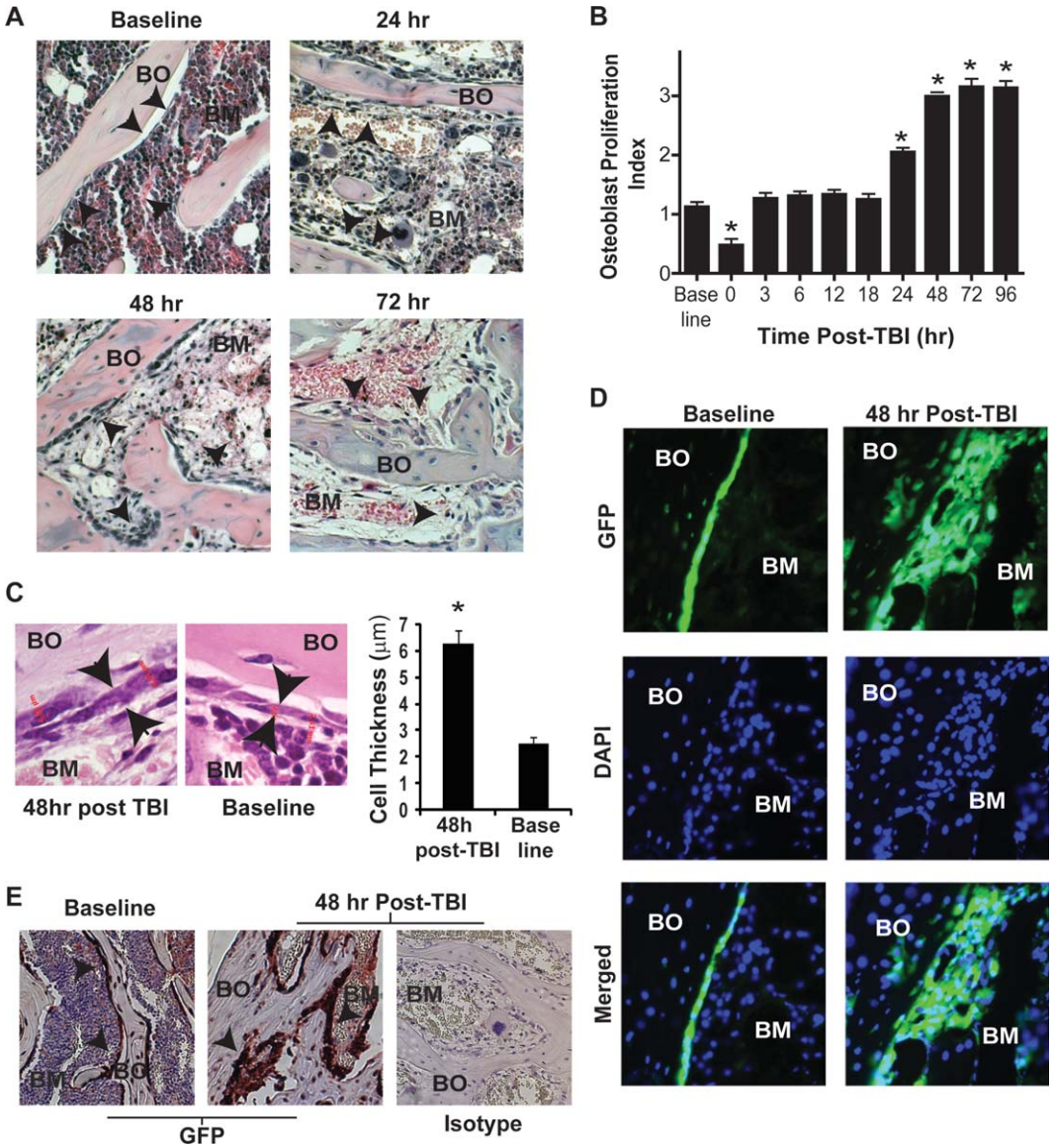

Figure 1. Time course of endosteal osteoblast expansion following TBI. **(A):** Representative H+E stained sections of BO and BM and **(B)** quantitative analysis (mean ± SEM, 8–10 mice each time point) showing the time course of endosteal osteoblast expansion following radioablation (1,125 cGy). *, $p < .01$ versus baseline. **(C):** Representative H+E stained sections and quantitative assessment (mean ± SEM, three sections/mouse, three mice/group) of individual osteoblast thickness at baseline and 48 hours after TBI. *, $p = .0001$ versus baseline. **(D):** Immunofluorescent staining (GFP, green; DAPI, blue) and **(E)** immunohistochemistry staining (GFP stained brown, black arrowheads) of BO/BM sections before and 48 hours after TBI, taken from COL2.3GFP mice, showing the marked increase in GFP^+ mature osteoblasts at the endosteal surface 48 hours after TBI. Abbreviations: BM, bone marrow; BO, bone; GFP, green fluorescent protein; TBI, total body irradiation.

Clustered Proliferative Endosteal Cells Drive Niche Expansion

To further define mechanisms driving osteoblast expansion after radioablation, we focused on the endosteal region of trabecular bone, staining sections for Ki-67 expression, a recognized cell proliferation marker [25]. Ki-67 expression in endosteal cells of trabecular bone was minimal up to 3 hours after TBI (data not shown). However, by 6 hours post-TBI, isolated cells and small clusters along the metaphyseal bone surface began to express Ki-67 (Fig. 2A, upper left panel) and, from 24 to 48 hours post-TBI, Ki-67 expression by osteoblasts was widespread and prominent (Fig. 2A, upper middle and right panels). To further confirm active proliferation of endosteal osteoblasts after irradiation, mice were also injected once with BrdU (bromodeoxyuridine) following irradiation. BrdU uptake was seen in discrete, isolated small groups of endosteal lining cells beginning 6 hours post-TBI and $BrdU^+$ cells significantly increased in clusters by 24 hours post-TBI (Fig. 2A, bottom left and middle panels). At 48 hours after irradiation, as expected, the number of BrdU-labeled cells declined (Fig. 2A, bottom right panels) suggesting that the cells that originally incorporated BrdU, at 24 hours post-TBI, continued to proliferate.

Together, these data suggested that post-TBI osteoblast expansion may have arisen from a small subset of osteoblasts with high proliferative potential, analogous to colony-forming units (CFUs) characteristic of primitive hematopoietic progenitors and mesenchymal cells. To test this

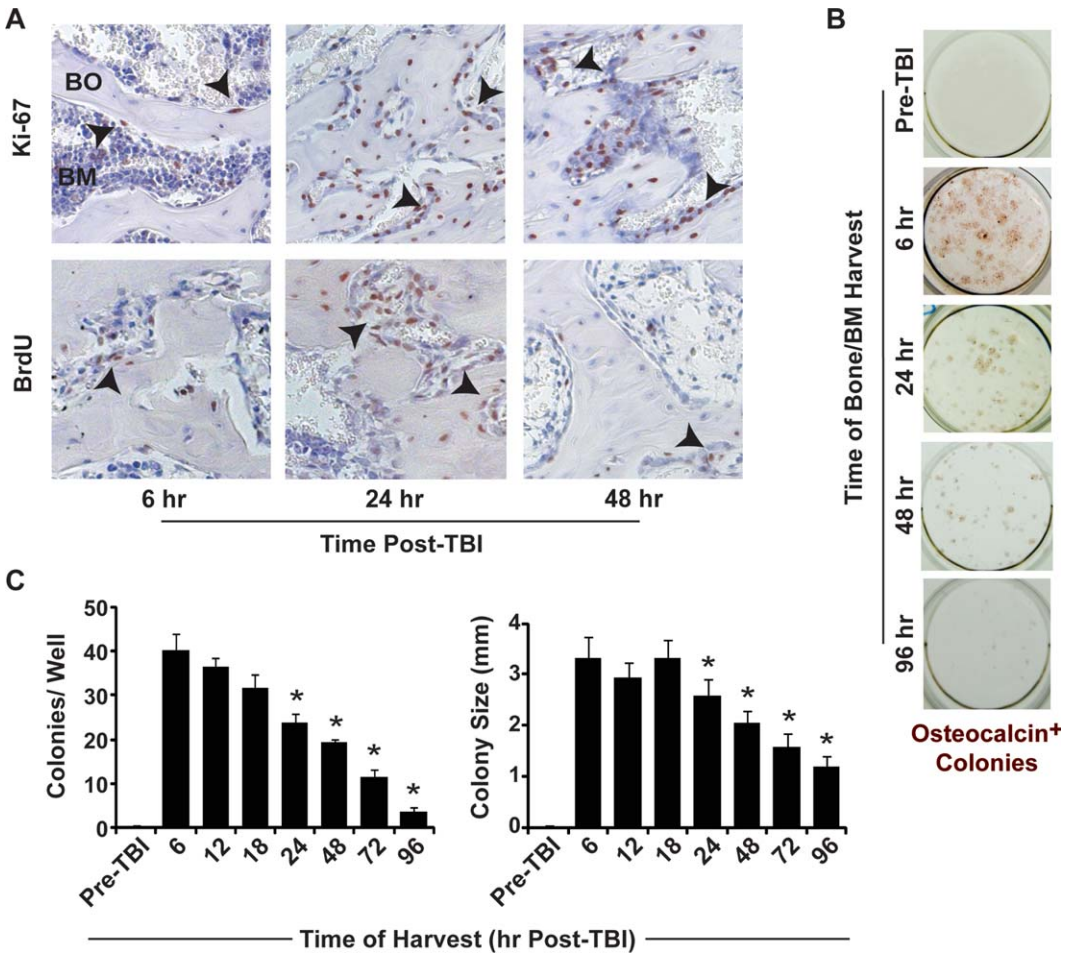

Figure 2. TBI-induced endosteal niche expansion arises from an osteoblast subset with high proliferative potential. **(A):** Immunostaining demonstrating expression of Ki-67 (brown-stained cells [arrowheads], upper panels) and BrdU incorporation (brown-stained cells [arrowheads], lower panels) in metaphyseal endosteal osteoblasts at 6, 24, and 48 hours after TBI. **(B):** Representative adherent cell culture colony growth, stained at 7 days for osteocalcin$^+$ osteoblasts, from BM and endosteal surface cells harvested from mice before and 6, 24, 48, and 96 hours post-TBI. **(C):** Quantitative analysis (mean ± SEM) of colony number (left) and average colony size (right) in the adherent cell cultures at baseline and 6–96 hours post-TBI ($n \geq 5$ per group). *, $p < .01$ versus 6 hours post-TBI. Abbreviations: BM, bone marrow; BO, bone; TBI, total body irradiation.

hypothesis, we harvested BM and endosteal lining cells from mouse femurs either before TBI or from 6 to 96 hours post-TBI, cultured those cells for 7 days, and analyzed the number and size of osteocalcin$^+$ osteoblast colonies within those cultures (Fig. 2B, 2C). No significant osteoblast colonies formed in the hematopoietic/endosteal cell cultures taken from unirradiated mice, which was consistent with hematopoietic cell-induced suppression of osteoblast growth. However, cells harvested between 6 and 18 hours post-TBI formed 30–40 colonies per well with an average colony diameter of 3 mm, indicating a remarkable in vitro proliferation of the CFU-initiating cells. From 6 to 96 hours post-TBI, the colony-forming potential of these cells progressively and significantly declined, with a 90% reduction in colony formation at 24, 48, 72, and 96 hours compared to that seen 6 hours post-TBI ($p < .01$ by one-way ANOVA). In addition, the size of colonies significantly decreased after TBI ($p < .01$ by one-way ANOVA), becoming 65% smaller than the average colony size seen at 6 hours post-TBI. These in vitro data strongly support the hypothesis that this in vivo increase of endosteal cells following TBI occurs through a proliferation program mediated initially by a select subset of proliferative osteoblasts.

Growth Factor Expression and Hematopoietic Cell Regulation of Osteoblastic Niche Expansion

Many growth factors, including PDGF-BB, TGFβ, bFGF, and IGF-1 are critical regulators of osteoblast growth and differentiation during normal development [26–28]. In turn, osteoblasts secrete the chemokine SDF-1 that serves as a potent chemoattractant, activating signal, and antiapoptotic factor for a variety of hematopoietic cells including HSC [29]. We analyzed the expression of these growth factors before TBI and during the osteoblast expansion response post-TBI (Fig. 3A). The time course analyses of protein (Fig. 3A) and mRNA (Fig. 3B) expression revealed a progressive and significant increase of SDF-1, PDGF-BB, bFGF, TGFβ, and IGF-1 ($p < .05$ for protein expression and $p \leq .01$ for mRNA expression by one-way ANOVA) of up to threefold by 48 hours post-TBI, compared to unirradiated BM levels. Interestingly, the increased expression of each of these growth factors correlated temporally with the expansion of the osteoblastic niche, shown earlier (Fig. 1B).

We then specifically focused on IGF-1 as a potential critical mediator involved in TBI-induced osteoblast expansion, as IGF-1 is a potent mediator of osteoblast proliferation [18] and may have a general role in niche regulation [30].

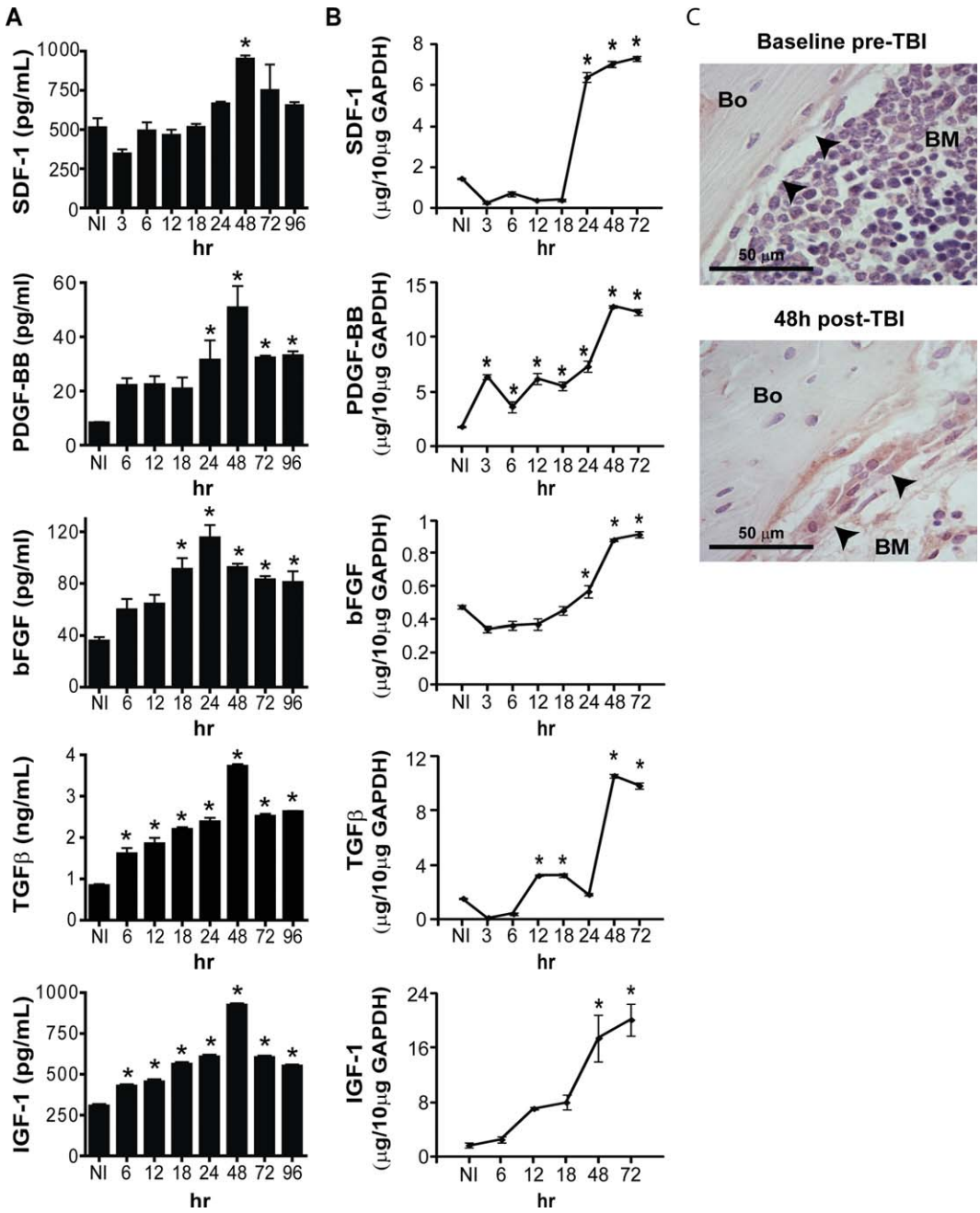

Figure 3. Osteoblast growth factor expression following TBI. **(A):** Protein expression (normalized per BM cell, mean ± SEM) of SDF-1, PDGF-BB, bFGF, TGFβ, and IGF-1 in BM isolated from either unirradiated (NI) or 3–96 hours post-TBI WT mice (n = 3–5 mice/time point). *, $p \leq .01$ versus expression in NI group. **(B):** qPCR analysis of SDF-1, PDGF-BB, bFGF, TGFβ, and IGF-1 relative mRNA (normalized to GAPDH) expression in BM cells isolated from unirradiated or 3–72 hours post-TBI WT mice (mean ± SD, n = 3 per time point, except IGF-1 data expressed as mean ± SEM, n = 2–6 per time point). *, $p \leq .01$ versus expression in NI group. **(C):** Representative immunostained BO and BM sections demonstrating increased expression of IGF-1 (brown-red-stained cells, arrowheads) at the metaphyseal endosteum at 48 hours post-TBI (bottom) versus baseline (top). Abbreviations: bFGF, basic fibroblast growth factor; BM, bone marrow; BO, bone; IGF-1, insulin-like growth factor 1; PDGF, platelet-derived growth factor; TBI, total body irradiation; TGFβ, transforming growth factor beta.

Immunohistochemical staining for BM IGF-1 expression performed at 48 hours post-TBI revealed increased expression compared to that seen in unirradiated controls (Fig. 3C), with the highest level of expression localized to endosteal osteoblasts, suggesting that a substantial fraction of the increased marrow IGF-1 (Fig. 3A, 3B) may arise from osteoblast secretion.

We next postulated that the endosteal osteoblast proliferation and increased expression of growth factors might be due to the absence of tonic inhibitory signals provided by hematopoietic cells, and specifically by primitive marrow cells demarcated by Sca-1$^+$ expression. To test this hypothesis, we compared osteoblast niche expansion at 48 hours post-TBI in mice receiving whole BMT immediately after TBI versus irradiated but not transplanted mice. In contrast to mice receiving TBI only (Fig. 4A, left), mice receiving whole BMT immediately after TBI (Fig. 4A, middle) did not exhibit significant osteoblastic niche expansion by 48 hours post-TBI, showing

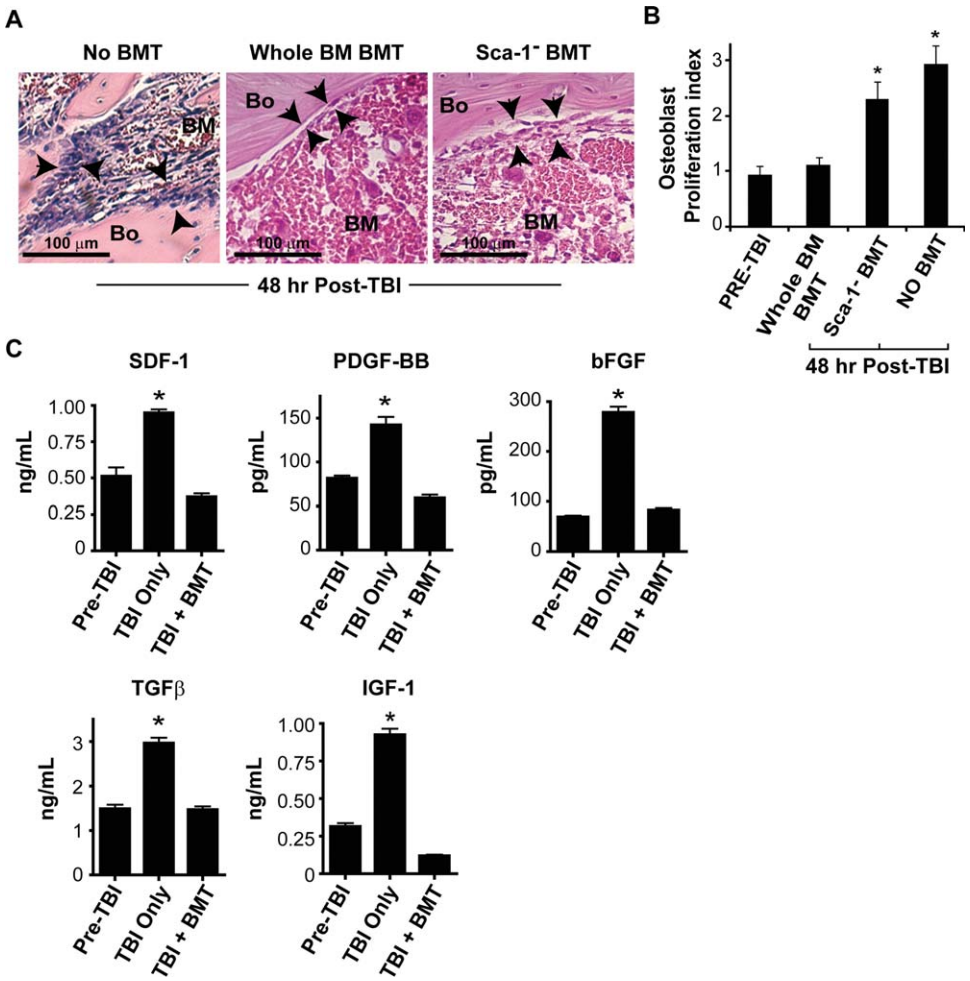

Figure 4. Early BMT following TBI prevents osteoblast niche expansion. **(A):** H+E stained BO and BM sections and **(B)** quantitative scoring analysis (right) comparing endosteal osteoblast expansion at baseline (Pre-TBI) and 48 hours post-TBI (left) in mice receiving (immediately after irradiation) either BMT with whole BM (3×10^6 cells), BMT with Sca-1$^+$ cell-depleted BM (3×10^6 cells), or no BMT. *, $p < .05$ versus pre-TBI and whole BM BMT groups. **(C):** SDF-1, PDGF-BB, bFGF, TGFβ, and IGF-1 protein expression in isolated BM cells harvested from unirradiated mice (pre-TBI), mice 48 hours post-TBI with no other treatment (TBI only), and mice 48 hours post-TBI who received 3×10^6 whole BM cells immediately after TBI (TBI + BMT) (n = 3–5 per group). *, $p < .001$ versus pre-TBI or TBI + BMT groups. Abbreviations: BM, bone marrow; BMT, bone marrow transplantation; BO, bone; IGF-1, insulin-like growth factor 1; TBI, total body irradiation; TGFβ, transforming growth factor beta.

only a single layer of endosteal cells, as in the controls prior to irradiation (Fig. 4B, significantly decreased vs. no BMT group, $p < .05$ by one-way ANOVA). However, irradiated mice who received Sca-1$^+$ cell-depleted BM immediately after TBI (Fig. 4A, right) still developed osteoblastic niche expansion similar to that seen after 48 hours post-TBI in nontransplanted mice (significantly increased vs. pre-TBI and whole BM BMT groups, $p < .05$ by one-way ANOVA), suggesting that the Sca-1$^+$ fraction of transplanted marrow cells, which contains HSCs and progenitors, prevents or rapidly reverses endosteal osteoblast expansion. Furthermore, in contrast to the marked increased expression of SDF-1, PDGF-BB, TGFβ, bFGF, and IGF-1 by BM cells at 48 hours post-TBI (Figs. 3A, 4C) relative to baseline pre-TBI levels, BM expression of these cytokines at 48 hours post-TBI in mice receiving BMT immediately after TBI (Fig. 4C) was less than or equal to baseline pre-TBI expression levels (significantly decreased from TBI only groups, $p < .001$ by one-way ANOVA). Collectively, these data suggest that Sca-1$^+$ cells negatively regulate the reversible BM niche reorganization after TBI and BMT.

Hematopoietic Cell Homing and HSC Engraftment Following BMT Are Enhanced by Radioablation-Induced Osteoblast Proliferation

Based on the observation that BM Sca-1$^+$ hematopoietic cells appear to play a regulatory role in osteoblastic niche expansion/reversion after BMT, we next sought to determine whether the expansion itself could represent a compensatory mechanism designed to improve homing and engraftment of HSCs in response to a sensed loss of BM. We performed initial BM homing assays using a GFP$^+$ transgenic mouse as a BM donor and WT mice as BMT recipients. BMT performed 48 hours post-TBI, the time of maximal osteoblast niche expansion resulted in a trend toward greater initial GFP$^+$ donor cell homing to BM within the first 6 hours post-BMT than homing seen when BMT was performed either immediately (0 hour) or 24 hours after TBI (Fig. 5A), although this trend did not reach statistical significance ($p = .20$). Strikingly, BM engraftment of GFP$^+$ donor cells, measured 24 hours after BMT (Fig. 5B), significantly increased in mice

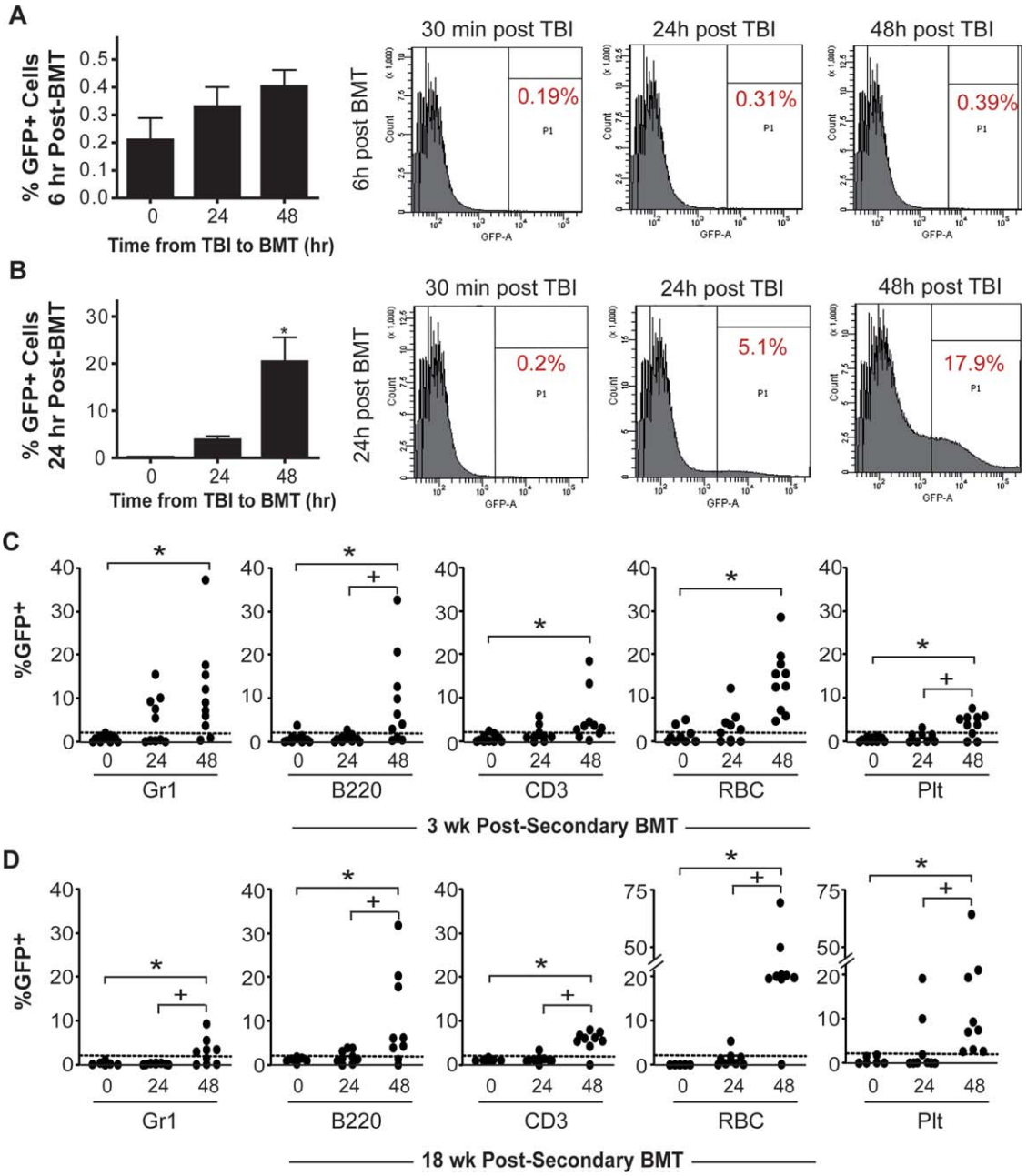

Figure 5. Maximal osteoblastic niche expansion increases initial donor cell homing to bone marrow (BM) and durable long-term hematopoietic stem cell/progenitor engraftment. **(A):** Donor GFP^+ cell homing to BM, expressed as the percentage of live GFP^+ BM cells (mean ± SEM, $n = 4$ mice per group), at 6 and **(B)** 24 hours post-BMT in WT mice receiving 3×10^6 GFP^+ whole BM cells either 0, 24, or 48 hours after TBI, with representative histograms shown for each group. *, $p < .05$ versus immediately (0 hours) or 24 hours post-TBI. **(C, D):** Competitive repopulation secondary transplantation assay in which primary (1°) recipient WT mice were transplanted with 3×10^6 GFP^+ whole BM at 0, 24, or 48 hours post-TBI. 1° recipient BM was then harvested at 24 hours post-1° BMT and transplanted into WT secondary (2°) recipient mice with 2×10^5 unirradiated WT whole BM competitor cells. Data are expressed as the percentage of GFP^+ cells in each peripheral blood lineage ($GR1^+$ myeloid cells, $B220^+$ B cells, $CD3^+$ T cells, RBC, or platelets) in 2° recipient mice at 3 weeks (C) and 18 weeks (D) post-2° BMT. Significantly increased GFP^+ 2° recipients (>2% GFP^+ cells, dashed line) in indicated blood cell lineage versus 0 hour (*, $p < .05$) or 24 hour ($^+$, $p < .05$) groups. Abbreviations: BMT, bone marrow transplantation; GFP, green fluorescent protein; TBI, total body irradiation.

transplanted 48 hours after TBI versus mice transplanted either immediately or 24 hours after TBI by 20- and 14-fold, respectively ($p \leq .05$ by one-way ANOVA).

To assess whether osteoblast niche expansion specifically enhances HSC engraftment, we performed a competitive repopulation secondary transplantation assay, in which GFP^+ BM was transplanted into WT primary (1°) recipient mice at variable times post-TBI, selected on the basis of the expansion time course data presented in Figure 1B. We performed 1° BMT either immediately (0 hour) after TBI when no osteoblastic niche expansion had occurred, at 24 hours post-TBI when niche expansion was beginning, or 48 hours post-TBI when expansion reached near maximal levels. In this assay, 24 hours after 1° BMT, BM was harvested from 1° recipients

and transplanted with competitor BM cells into irradiated secondary (2°) recipient mice. Thus, the percentage of 2° recipients with GFP^+ hematopoiesis, defined as >2% GFP^+ cells within peripheral blood RBC, platelet, myeloid cell, and lymphocyte lineages, directly reflects HSC engraftment efficiency in 1° recipients transplanted either immediately (0 hour), 24 hours, or 48 hours post-TBI.

At 3 weeks post-2° recipient BMT (Fig. 5C), when most hematopoiesis was derived from short-term (ST)-HSC or progenitor cells, GFP^+ hematopoietic reconstitution within each lineage increased more than fivefold in 2° recipients of BM from 1° recipients transplanted 48 hours post-TBI versus immediately after TBI ($p < .05$ by Fisher's Exact test), demonstrating significantly increased ST-HSC and progenitor engraftment efficiency when BMT was performed at the time of maximal osteoblast niche expansion.

At 18 weeks post-2° BMT (Fig. 5D), when hematopoiesis is solely dependent upon LT-HSC engraftment, 2° recipients of BM from 1° recipients that received BMT immediately after TBI had no significant GFP^+ cell engraftment, whereas the majority of 2° recipients whose BM came from 1° recipients transplanted 48 hours post-TBI retained significant GFP^+ reconstitution of RBC, platelet, myeloid, and lymphocyte lineages ($p < .05$ vs. 0 and 24 hour groups by Fisher's Exact test). These data demonstrate that LT-HSC engraftment significantly increased when BMT was performed at the time of maximal niche expansion.

IGF-1 Signaling Blockade Disrupts Both Radioablation-Induced Osteoblastic Niche Expansion and Efficient HSC Engraftment Following BMT

IGF-1 is crucial for skeletal bone development [18] and, indirectly, for the developmental formation of the endosteal niche [31]. Moreover, IGF-1 plays a role in the regulatory niche of pluripotent stem cells [30]. Thus, having identified a striking increase in marrow IGF-1 after radioablation concomitant with endosteal niche expansion and HSC engraftment (Figs. 3A, 3B, 4C), we hypothesized that this cytokine may be a key regulator of the HSC endosteal niche. To test this idea, we treated mice with picropodophyllin (PPP), a potent and selective IGF-1 receptor tyrosine kinase inhibitor [32] with a short half-life ($t_{1/2} \sim 3$ hours). PPP was administered just before TBI and again 12 hours after TBI. At 48 hours post-TBI, we observed a nearly complete abrogation of TBI-induced osteoblast expansion (Fig. 6A).

We then performed an additional competitive repopulation 2° transplantation assay similar to that described above, testing irradiated 1° recipients that received either no other treatment, IGF-1 signaling inhibition using PPP, or sham vehicle (dimethyl sulfoxide) treatment at the time of TBI. Once again, using GFP^+ reconstitution of 2° recipients at 3 weeks and 18 weeks as a measure of 1° recipient ST-HSC/progenitor and LT-HSC engraftment efficiency, respectively, we found that both ST-HSC (Fig. 6B; *, $p < .05$ by Fisher's Exact test) and LT-HSC (Fig. 6C; *, $p < .05$ by Fisher's Exact test) engraftment were severely diminished when osteoblast niche expansion was blocked by PPP-mediated IGF-1 signaling inhibition. Intravenous infusion of IGF-1 at the time of TBI, however, did not enhance osteoblast expansion or stem cell engraftment (Supporting Information Fig. S3), most likely because either the concentration of the systemically infused IGF-1 in the marrow microenvironment was insufficient or physiologic osteoblast niche expansion is maximal. Nonetheless, these findings further confirm the critical importance of osteoblast niche expansion following TBI in the facilitation of stem cell engraftment, and they identify IGF-1-driven signaling as a critical direct mediator of TBI-induced niche expansion and an indirect mediator of HSC engraftment.

Discussion

Our data demonstrate that the remarkable reorganization of the endosteal niche following radioablation that we described previously [16] consists of expansion of proliferating endosteal osteoblasts and serves critical functions for donor hematopoietic cell homing and both short-term and LT-HSC engraftment in the recipient BM space following BMT. Moreover, we have begun to elucidate cellular and molecular pathways inherent in this niche response, demonstrating that signaling through the IGF-1 receptor drives proliferation of mature osteoblasts from a small subset of primitive mesenchymal progenitors with high proliferative potential. The ability to block hematopoietic cell engraftment by inhibition of IGF-1-mediated niche expansion provides compelling evidence for the key role of endosteal niche expansion in facilitating efficient HSC engraftment. Moreover, complete elucidation of the molecular and cellular pathways of the niche reorganization may provide novel targets to enhance HSC engraftment in clinical transplantation. Exploiting such strategies would be invaluable in the setting of limited stem cell doses, such as increasingly used cord blood transplantation methods as well as in HSC transplantation for diseases that are biologically resistant to engraftment.

The specific signal that triggers the initiation of post-TBI osteoblastic niche expansion remains unknown. One possibility is that direct radiation toxicity to the mesenchymal niche elements, including osteoblasts, could initiate this reorganization as a damage-repair mechanism. However, the expanded niche post-TBI vastly exceeds the number of niche elements present at baseline, and it is rare for this type of overcorrection to occur in physiologic repair mechanisms. Our data showing that early transplantation following TBI with whole BM, but not $Sca\text{-}1^+$ cell-depleted BM, can rapidly reverse or possibly block niche expansion and the associated increased expression of mesenchymal growth factors suggest that disruption of crosstalk between $Sca\text{-}1^+$ hematopoietic cells and the endosteal niche cells initiates the observed osteoblast expansion program. Hematopoietic cells within the $Sca\text{-}1^+$ fraction may actively suppress osteoblast proliferation, or conceivably, HSC occupancy of the endosteal niche after BMT may regulate osteoblast proliferation through adhesion molecules or signaling. Interruption of these interactions by marrow ablation may release the restraint that leads to osteoblast proliferation. From a teleological perspective, such a mechanism may have evolved as a survival mechanism to maintain and recruit HSCs within the niche following infectious or environmental exposures that cause HSC toxicity. Thus, the cellular reorganization may be viewed as an activation of the endosteal niche to bind circulating HSCs and reestablish hematopoiesis after environmental injury.

Based on our Ki-67 and BrdU immunostaining assays, post-TBI niche expansion originates in a few relatively radioresistant high proliferative potential cells. Our in vitro colony assays demonstrated that these progenitors undergo colony-type proliferation beginning soon after TBI, giving rise primarily to maturing osteoblasts, as demonstrated in our in vivo Col2.3GFP mouse model, in which only mature osteoblasts express GFP [20,21]. Although the majority of the increased population of endosteal cells post-TBI in this model are GFP^+ osteoblasts, a small percentage are GFP^-, suggesting that other mesenchymal cell types also known to play critical

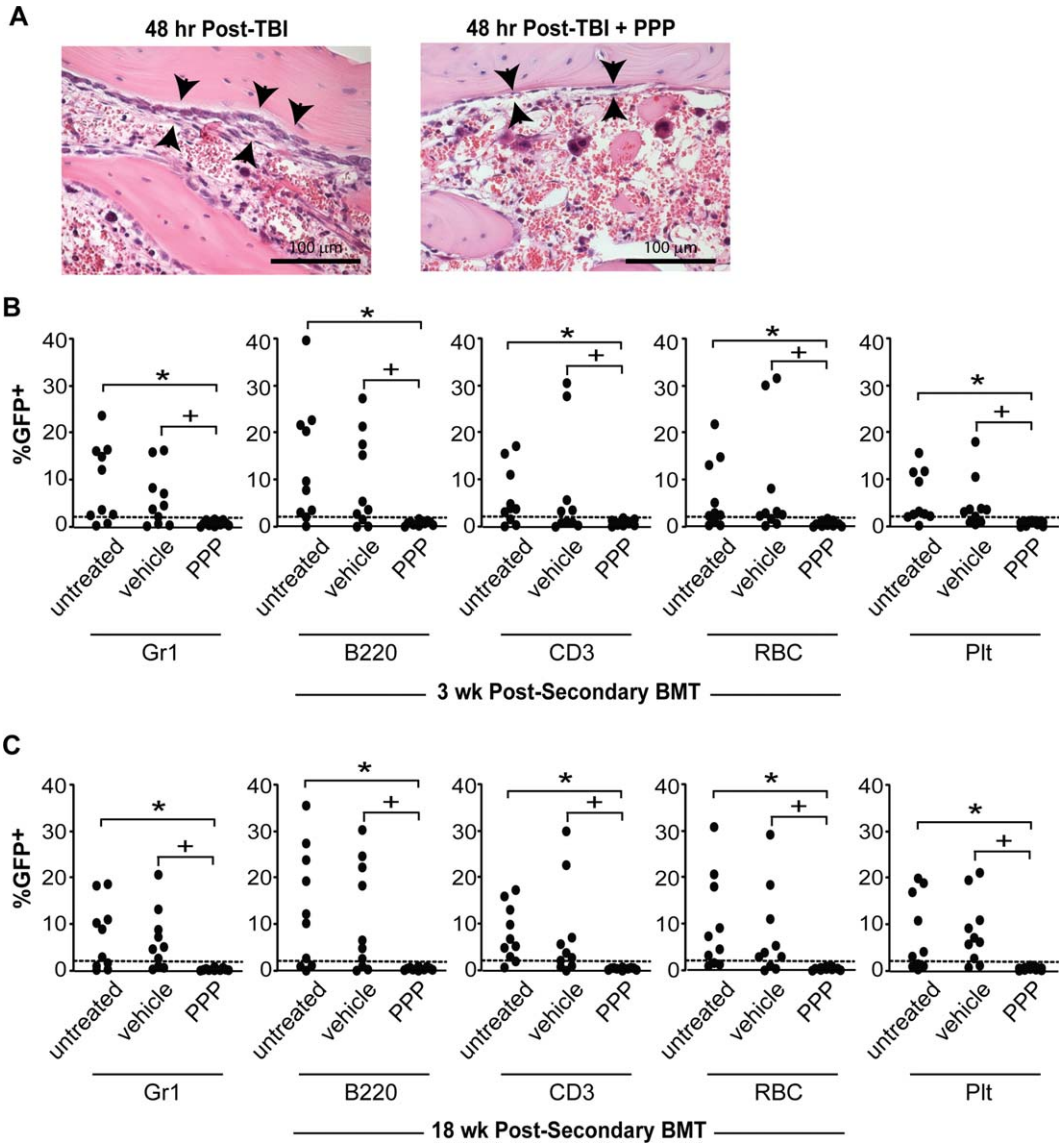

Figure 6. Blockade of insulin-like growth factor 1 (IGF-1) signaling disrupts both TBI-induced osteoblast proliferation and hematopoietic stem cell engraftment following bone marrow (BM). **(A):** H+E stained BM sections demonstrating marked reduction in 48 hour post-TBI osteoblast niche expansion (arrowheads) in WT mice receiving TBI and the IGF-1-receptor tyrosine kinase inhibitor PPP (20 mg/kg) (right) versus mice receiving TBI only (left). **(B, C):** Competitive secondary (2°) transplantation assay in which untreated, vehicle-treated (DMSO), or PPP-treated primary (1°) recipient mice received BMT (3×10^6 GFP^+ whole BM cells) at 48 hours post-TBI, and competitive 2° BMT was performed 24 hours after 1° BMT with 1° recipient BM and 2×10^5 unirradiated WT BM cells. Data reflect the percentage of GFP^+ cells in specified peripheral blood lineages at 3 weeks (B) and 18 weeks (C) post-2° BMT in 2° recipients of untreated, vehicle-treated, or PPP-treated primary recipient BM. Significantly decreased GFP^+ 2° recipients (>2% GFP^+ cells, dashed line) in indicated blood cell lineage versus untreated (*, $p < .02$) or vehicle-treated ($^+$, $p < .05$) groups. Abbreviations: BMT, bone marrow transplantation; GFP, green fluorescent protein; PPP, picropodophylin; TBI, total body irradiation.

roles in homeostatic niche function [33] must also be present in the expanded endosteal microenvironment post-TBI. Thus, although mature osteoblasts are the predominant population within the niche post-TBI, the relative contributions of bone-generating osteoblasts versus other minority niche elements post-TBI in providing specific HSC binding sites and/or functionally enabling engraftment require further study.

The kinetics of niche expansion following TBI appears to be strain-dependent, as osteoblast expansion in the C57BL/6 mice used in this study occurred faster than we previously observed in FVB/N mice [16]. Such murine strain variation in niche expansion may be related to strain-dependent mesenchymal proliferation capacity, which we previously reported [34]. The kinetics of our C57BL/6 model have the advantage of allowing us to comparatively investigate HSC homing and engraftment at times of no expansion (immediately after TBI), 50% expansion (24 hours post-TBI), and >95% (maximal) expansion (48 hours post-TBI). This comparison demonstrates clear superiority of HSC engraftment efficiency when BMT is performed at 48 hours post-TBI, the time of maximal osteoblast expansion. Whether an osteoblastic niche expansion response exists in human subjects undergoing BMT after radioablation and whether it follows similar kinetics remains unknown. Thus, optimization of clinical BMT timing in

relation to radioablation and its initiation of niche proliferation would require large-animal studies or human-subject translational research.

Our novel finding that IGF-1 signaling is required for TBI-induced niche osteoblast proliferation and subsequent measurable HSC engraftment in our model is consistent with the well-described essential role that IGF-1 plays in modulating osteoblast growth during development and under homeostatic conditions [35]. IGF-1 signaling inhibition with PPP, a specific small-molecule inhibitor with a short half-life ($t_{1/2} \sim$ 3 hours) [32], could not have directly affected the transplanted donor hematopoietic cells, given that the final dose was administered 36 hours before transplantation. Thus, our model allows us to test the effects of inhibiting IGF-1 in the BM microenvironment, or elsewhere within the host, without affecting IGF-1-dependent pathways in donor HSC. Osteoblasts produce IGF-1, which influences growth through both paracrine and autocrine pathways [28]. IGF-1 is also an essential downstream mediator of parathyroid hormone effects on osteoblast growth [36]. Thus, the previously reported increase in baseline HSC in mice with transgenic osteoblast-specific parathyroid hormone receptor upregulation [4] may also rely upon IGF-1 signaling. Additionally, IGF-1 is also known to stimulate osteoblast secretion of vascular endothelial growth factor (VEGF) [37], and thus may also play a role in VEGF receptor-2 signaling previously shown to be required for hematopoietic reconstitution following BMT [9].

Conclusion

In sum, we have shown that endosteal niche expansion following radioablation reflects proliferation of mature osteoblasts from relatively infrequent radio-resistant cells in a time course that parallels the expression of osteoblast growth factors. HSC engraftment efficiency is superior when BMT is performed during maximal osteoblast expansion. IGF-1 signaling blockade completely abrogates both osteoblast niche expansion as well as measureable HSC engraftment following transplantation. Taken together, our data demonstrate the critical importance of IGF-1-driven reorganization of the BM microenvironment, and specifically the osteoblastic niche, in enabling efficient HSC engraftment following transplantation. Further understanding of these niche expansion pathways will allow identification of therapeutic strategies to improve HSC engraftment in the clinical BMT setting.

Acknowledgments

We gratefully acknowledge Dr. Alan Flake for provision of flow cytometry. This work was supported in part by the Grants NIH R01 HL077643 (EMH), T32HL007150-34, NHLBI 2 K12 HL087064, and the 2011 American Society of Hematology Research Training Award for Fellows (TSO). TSO and EMH are also supported by the Canuso Foundation Innovation Grant. We also acknowledge grants from the Ministero della Salute Bando Cellule Staminali, the Regione Emilia Romagna, the Associazione per il Sostegno dell'Ematologia e dell'Oncologia Pediatrica (ASEOP), and Fondazione Cassa di Risparmio di Modena (AC and MD).

Disclosure of Potential Conflicts of Interest

The authors indicate no potential conflict of interest.

References

1 Fuchs E, Tumbar T, Guasch G. Socializing with the neighbors: Stem cells and their niche. Cell 2004;116:769–778.
2 Li L, Xie T. Stem cell niche: Structure and function. Annu Rev Cell Dev Biol 2005;21:605–631.
3 Adams GB, Scadden DT. The hematopoietic stem cell in its place. Nat Immunol 2006;7:333–337.
4 Calvi LM, Adams GB, Weibrecht KW et al. Osteoblastic cells regulate the haematopoietic stem cell niche. Nature 2003;425:841–846.
5 Zhang J, Niu C, Ye L et al. Identification of the haematopoietic stem cell niche and control of the niche size. Nature 2003;425:836–841.
6 Garrett RW, Emerson SG. Bone and blood vessels: The hard and the soft of hematopoietic stem cell niches. Cell Stem Cell 2009;4:503–506.
7 Moore KA, Lemischka IR. Stem cells and their niches. Science 2006; 311:1880–1885.
8 Slayton WB, Li XM, Butler J et al. The role of the donor in the repair of the marrow vascular niche following hematopoietic stem cell transplant. Stem Cells 2007;25:2945–2955.
9 Hooper AT, Butler JM, Nolan DJ et al. Engraftment and reconstitution of hematopoiesis is dependent on VEGFR2-mediated regeneration of sinusoidal endothelial cells. Cell Stem Cell 2009;4:263–274.
10 Yoshihara H, Arai F, Hosokawa K et al. Thrombopoietin/MPL signaling regulates hematopoietic stem cell quiescence and interaction with the osteoblastic niche. Cell Stem Cell 2007;1:685–697.
11 Taichman RS, Reilly MJ, Emerson SG. Human osteoblasts support human hematopoietic progenitor cells in vitro bone marrow cultures. Blood 1996;87:518–524.
12 Askmyr M, Sims NA, Martin TJ et al. What is the true nature of the osteoblastic hematopoietic stem cell niche? Trends Endocrinol Metab 2009;20:303–309.
13 Visnjic D, Kalajzic Z, Rowe DW et al. Hematopoiesis is severely altered in mice with an induced osteoblast deficiency. Blood 2004; 103:3258–3264.
14 Lo Celso C, Fleming HE, Wu JW et al. Live-animal tracking of individual haematopoietic stem/progenitor cells in their niche. Nature 2009;457:92–96.
15 Xie Y, Yin T, Wiegraebe W et al. Detection of functional haematopoietic stem cell niche using real-time imaging. Nature 2009;457:97–101.
16 Dominici M, Rasini V, Bussolari R et al. Restoration and reversible expansion of the osteoblastic hematopoietic stem cell niche after marrow radioablation. Blood 2009;114:2333–2343.
17 Greenbaum A, Hsu YM, Day RB et al. CXCL12 in early mesenchymal progenitors is required for haematopoietic stem-cell maintenance. Nature 2013;495:227–230.
18 Govoni KE, Wergedal JE, Florin L et al. Conditional deletion of insulin-like growth factor-I in collagen type 1alpha2-expressing cells results in postnatal lethality and a dramatic reduction in bone accretion. Endocrinology 2007;148:5706–5715.
19 Dominici M, Tadjali M, Kepes S et al. Transgenic mice with pancellular enhanced green fluorescent protein expression in primitive hematopoietic cells and all blood cell progeny. Genesis 2005;42:17–22.
20 Dacic S, Kalajzic I, Visnjic D et al. Col1a1-driven transgenic markers of osteoblast lineage progression. J Bone Miner Res 2001;16: 1228–1236.
21 Kalajzic I, Kalajzic Z, Kaliterna M et al. Use of type I collagen green fluorescent protein transgenes to identify subpopulations of cells at different stages of the osteoblast lineage. J Bone Miner Res 2002;17:15–25.
22 Szilvassy SJ, Ragland PL, Miller CL et al. The marrow homing efficiency of murine hematopoietic stem cells remains constant during ontogeny. Exp Hematol 2003;31:331–338.
23 Katayama Y, Battista M, Kao WM et al. Signals from the sympathetic nervous system regulate hematopoietic stem cell egress from bone marrow. Cell 2006;124:407–421.
24 Lee-Thedieck C, Rauch N, Fiammengo R et al. Impact of substrate elasticity on human hematopoietic stem and progenitor cell adhesion and motility. J Cell Sci 2012;125:3765–3775.
25 Urruticoechea A, Smith IE, Dowsett M. Proliferation marker Ki-67 in early breast cancer. J Clin Oncol 2005;23:7212–7220.

26 Hock JM, Canalis E. Platelet-derived growth factor enhances bone cell replication, but not differentiated function of osteoblasts. Endocrinology 1994;134:1423–1428.
27 Jackson RA, Nurcombe V, Cool SM. Coordinated fibroblast growth factor and heparan sulfate regulation of osteogenesis. Gene 2006;379:79–91.
28 Gabbitas B, Canalis E. Insulin-like growth factors sustain insulin-like growth factor-binding protein-5 expression in osteoblasts. Am J Physiol 1998;275:E222–228.
29 Lataillade JJ, Clay D, Bourin P et al. Stromal cell-derived factor 1 regulates primitive hematopoiesis by suppressing apoptosis and by promoting G(0)/G(1) transition in CD34(+) cells: Evidence for an autocrine/paracrine mechanism. Blood 2002;99:1117–1129.
30 Bendall SC, Stewart MH, Menendez P et al. IGF and FGF cooperatively establish the regulatory stem cell niche of pluripotent human cells in vitro. Nature 2007;448:1015–1021.
31 Chan CK, Chen CC, Luppen CA et al. Endochondral ossification is required for haematopoietic stem-cell niche formation. Nature 2009;457:490–494.
32 Girnita A, Girnita L, del Prete F et al. Cyclolignans as inhibitors of the insulin-like growth factor-1 receptor and malignant cell growth. Cancer Res 2004;64:236–242.
33 Castillo AB, Jacobs CR. Mesenchymal stem cell mechanobiology. Curr Osteoporos Rep 2010;8:98–104.
34 Otsuru S, Hofmann TJ, Rasini V et al. Osteopoietic engraftment after bone marrow transplantation: Effect of inbred strain of mice. Exp Hematol 2010;38:836–844.
35 Canalis E. Growth factor control of bone mass. J Cell Biochem 2009; 108:769–777.
36 Miyakoshi N, Kasukawa Y, Linkhart TA et al. Evidence that anabolic effects of PTH on bone require IGF-I in growing mice. Endocrinology 2001;142:4349–4356.
37 Goad DL, Rubin J, Wang H et al. Enhanced expression of vascular endothelial growth factor in human SaOS-2 osteoblast-like cells and murine osteoblasts induced by insulin-like growth factor I. Endocrinology 1996;137:2262–2268.

See www.StemCells.com for supporting information available online.